# *A transient-flow syringe air permeameter*

GEOPHYSICS, VOL. 78, NO. 5 (SEPTEMBER-OCTOBER 2013); P. D307–D313, 5 FIGS.
10.1190/GEO2012-0534.1

# A transient-flow syringe air permeameter

Stephen Brown[1] and Martin Smith[2]

## ABSTRACT

In response to the need to better describe spatial variations in permeability, we designed and built a new portable field air permeameter for use on rocks in outcrop and core. In this instrument, a chamber containing a small volume of air in contact with the rock is suddenly increased in volume creating a vacuum, causing air to flow from the rock into the chamber. The instantaneous chamber volume and the air pressure within it were monitored. We evaluated a theory to allow interpretation of these data for the rock permeability. The theory required knowledge of some difficult-to-determine geometric constants. This difficulty was circumvented in practice through a calibration procedure. We described the theory for the design and construction of this instrument and reviewed some successful uses in field-scale studies of rock permeability heterogeneity.

## INTRODUCTION

Physical and chemical processes, including deposition, diagenesis, and mechanical deformation, create heterogeneity and anisotropy in rock and soil properties at all scales. Therefore, much recent effort has been placed on incorporating heterogeneity into numerical models of flow and transport and toward understanding how such effects upscale (Dagan, 1986; Koltermann and Gorelick, 1996).

In these studies, the primary physical parameters of interest are the spatial variability of permeability and porosity. Field studies indicate that permeability can vary several orders of magnitude over just a few meters at any particular site. Porosity can vary by more than one order of magnitude. Field studies also show that such spatially varying properties greatly influence subsurface flow and transport. Large-scale structures give rise to channelization, whereas large and small variations control solute spreading or dispersion (Koltermann and Gorelick, 1996).

The direct use of data measured at the finest scale is impractical for large geologic problems. Simplification and upscaling of this information are necessary. Yet, to understand the properties at the field scale, we must understand the magnitude of influences at the next-smallest scale. The mesoscale (pore-to-laboratory scale, i.e., submillimeter to meter) has been traditionally neglected, in spite of the fact that many coupled reactive transport processes, from radionuclide sorption to biologic attenuation, occur at this scale. To incorporate these mesoscale measurements into field-scale simulations, we must develop physically based upscaling procedures, which are built upon realistic descriptions of fine-scale heterogeneity. In this way, the effective properties at the largest scale remain self-consistent, and they are in agreement with well-established fundamental physics and chemistry processes operating at the smallest scales.

To fully develop and test such upscaling procedures, example data are required that have known permeability on a finely spaced spatial grid. In this paper, we describe the design and construction of a new portable field air permeameter instrument to measure the permeability of rocks in outcrop and on core.

## BACKGROUND: AIR PERMEAMETERS

In response to the need to better describe spatial variations in permeability, air permeameters have been developed and used in a wide variety of laboratory and field applications (e.g., Goggin et al., 1988a; Dreyer et al., 1990; Jacobsen and Rendall, 1991; Hartkamp et al., 1993; Tidwell and Wilson, 1999; Castle et al., 2004). Hurst and Goggin (1995) and Huysmans et al. (2008) provide concise histories and bibliographies of air permeameters.

Perhaps the first description of a device for obtaining small-scale air permeability measurements has been presented by Dykstra and Parsons (1950). A probe permeameter is usually constructed as a nozzle through which gas (nitrogen or air) can be released into a

Manuscript received by the Editor 20 December 2012; revised manuscript received 5 April 2013; published online 25 July 2013.
[1]Formerly New England Research, White River Junction, Vermont, USA; presently Massachusetts Institute of Technology, Cambridge, Massachusetts, USA. E-mail: delatierra@airpost.net.
[2]Formerly New England Research, White River Junction, Vermont, USA; presently Blindgoat Geophysics, Sharon, Vermont, USA. E-mail: martin@blindgoat.org.

porous medium. Gas leakage between the annulus of the nozzle and the porous medium is avoided by placing a ring of rubber or some other compressible, impermeable material in the interface between the probe and the medium. The gas-flow rate and gas pressure are monitored and can be transformed into gas permeability by empirically derived relationships or by use of an analytical equation, such as the modified form of Darcy's law including a geometrical factor depending on the tip seal size proposed in the seminal papers on probe permeameters by Goggin et al. (1988a, 1988b).

Disadvantages of air-permeability measurements of this type are the anticipated sensitivity of the response to partial or full saturation of the sample, sample surface effects such as irregularities and weathering, and the unknown geometry of flow paths from the probe into the medium. Limited knowledge of these effects will lead to uncertainty in data interpretation.

In detailed analysis of the use of probe permeameters, Goggin et al. (1988a, 1988b) have shown that for certain ranges of permeability, the simplest theory should be corrected to account for gas slippage and high-velocity gas flow effects. Furthermore, they estimated that the zone of investigation of a mini permeameter in an isotropic medium is a hemisphere of radius approximately four times the internal radius of the tip seal. More recently, Jensen et al. (1994) assert that probe permeameter measurements are even more localized with a depth of investigation of the order of only two probe inner radii.

## A SYRINGE AIR PERMEAMETER

The most obvious method to construct an air permeameter is to make use of Darcy's law and to combine a method to maintain constant air pressure across a specimen using a compressed gas storage tank and multiple pressure regulators with a series of gas-flow meters to measure the resulting air flow. A computerized data acquisition system would monitor the pressure/flow data and perform calculations to derive permeability. Similarly, a pressure-decay technique could be implemented with additional theory and physical components.

Many implementations of these techniques have resulted in bulky probe permeameter systems with limited transportability for field use. For example, Iversen et al. (2003) describe a device for studying spatial variability of soil permeability in the field. The device consists of a gas bottle, floating-ball-type gas flow meters, and a water-filled manometer for pressure measurements. We present an alternative implementation leading to a compact and transportable field instrument. We refer to this as a transient-flow syringe permeameter. The theory of operation and the implementation of this device are described below.

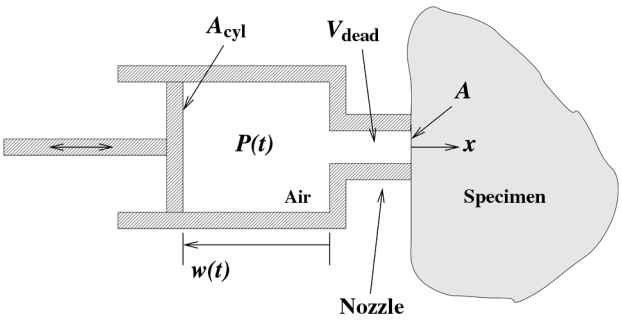


Figure 1. Schematic of the syringe air permeameter.

## Theory

A cylinder of area $A_{cyl}$ with a movable piston is filled with air (Figure 1). The cylinder is in contact with a specimen through a nozzle that has a cross-sectional area $A$ and a dead volume $V_{dead}$. As the piston moves, the internal pressure $P_0(t)$ and the piston displacement $w(t)$ are measured. The total air-filled volume of the system as a function of time is $V(t) = V_{dead} + A_{cyl} \times w(t)$. The coordinate system $(x, y, z)$ representing the position in the specimen has its origin at the specimen surface centered where the nozzle makes contact. As the piston moves, the pressure within the cylinder differs from that in the specimen. To compensate, air flows to or from the specimen at a rate controlled by the specimen permeability and the instantaneous pressure gradient at the nozzle ($x = 0$).

We can measure the cylinder volume $V$ and the air pressure (or vacuum) in the cylinder $P$ as a function of time $t$. If necessary, we could also measure the air temperature within the cylinder $T$ as a function of time. We now examine how the parameters $V(t)$, $P(t)$, and $T(t)$ are related to the air permeability $k$ of the specimen.

### *Pressure change in chamber*

First, we examine in detail the time rate of air pressure change in the chamber:

$$\frac{\partial P}{\partial t} = \underbrace{\frac{\partial P}{\partial V}\frac{\partial V}{\partial t}}_{\text{volume change}} + \underbrace{\frac{\partial P}{\partial T}\frac{\partial T}{\partial t}}_{\text{temperature change}} + \underbrace{\frac{\partial P}{\partial n}\frac{\partial n}{\partial t}}_{\text{moles of gas in or out}}. \quad (1)$$

### *Ideal gas law*

We assume that air is an ideal gas, and we make use of the ideal gas law, $PV = nRT$, to derive expressions for the partial derivatives in equation 1. Differentiating the ideal gas law for first term, we find

$$\frac{\partial P}{\partial V} = -\frac{nRT}{V^2} = -\frac{P}{V}. \quad (2)$$

However, thermodynamic considerations give the more general result (Zemansky, 1968):

$$\frac{\partial P}{\partial V} = -\gamma\frac{P}{V}, \quad (3)$$

where a new term $\gamma$ appears, the value of which depends upon whether the volume change is done under purely adiabatic or isothermal conditions. For adiabatic conditions, $\gamma = C_P/C_V$ is the ratio of the heat capacities at constant pressure and constant volume, respectively, which for nitrogen gas ($N_2$) at $P = 0$ is $\gamma \approx 1.4$. For isothermal conditions, $\gamma = 1$. Therefore, reasonable bounds for this parameter are $1 \le \gamma \le 1.4$.

Because equation 3 implicitly considers the effect of temperature change resulting from changes in volume or pressure (or at least the bounding cases thereof — from zero temperature change in the isothermal case to the maximum possible temperature change in the adiabatic case), and because in practice we do not expect significant external temperature changes to occur over the time scale of

our measurements, we drop the second term in equation 1 and we do not consider it further.

We must consider both parts of the third term in equation 1. Differentiating the ideal gas law for the first part, we find

$$\frac{\partial P}{\partial n} = \frac{RT}{V}. \tag{4}$$

We now consider the second part. Suppose that gas molecules enter the cylinder from the specimen. They will increase the pressure according to the ideal gas law. This can be thought of as an extra volume filled with gas being appended to the original cylinder, then the enlarged cylinder is sealed off and its contents are then reduced back to the original cylinder volume. To model this effect, we take the partial derivative $\partial n/\partial t$ in the ideal gas law considering $P$ and $T$ to be constant. In this step, we must distinguish between the total cylinder volume $V$ and the volume of the new gas molecules $V_{\text{gas}}$ at the current $P-T$ conditions. Therefore, we find

$$\frac{\partial n}{\partial t} = \frac{P}{RT}\frac{\partial V_{\text{gas}}}{\partial t}. \tag{5}$$

Combining equations 1, 3, 4, and 5 gives

$$\frac{\partial P}{\partial t} = -\gamma\frac{P}{V}\frac{\partial V}{\partial t} + \frac{P}{V}\frac{\partial V_{\text{gas}}}{\partial t} \tag{6}$$

or

$$\frac{V}{P}\frac{\partial P}{\partial t} + \gamma\frac{\partial V}{\partial t} = \frac{\partial V_{\text{gas}}}{\partial t}. \tag{7}$$

*Boundary conditions*

At the boundary of the sample, the flow of gas in or out of the cylinder is governed by Darcy's law,

$$Q = \frac{\partial V_{\text{gas}}}{\partial t} = -\frac{kA}{\mu}\nabla P|_{x=0}, \tag{8}$$

where $V_{\text{gas}}$ is the volume of gas at pressure $P$ and temperature $T$, $A$ is the area of the inlet for air flow to the cylinder at the sample boundary ($x = 0$), and $\mu$ is the viscosity of the gas. Combining equation 7 with equation 8, the relationship among the pressure and volume time histories and the permeability of the sample is

$$\frac{V}{P}\frac{\partial P}{\partial t} + \gamma\frac{\partial V}{\partial t} = -\frac{kA}{\mu}\nabla P|_{x=0}. \tag{9}$$

*Pressure gradient at the sample boundary*

We can measure complete time histories of pressure and cylinder volume throughout an experiment. We see from equation 9 that to estimate permeability, we need the pressure gradient at the sample boundary as a function of time as well. Fortunately, this is a tractable problem. Transient fluid flow follows the diffusion equation, which is analogous to the telegraph equation of electrical engineering. Wylie (1975) provides a clue to the solution of our problem in an example of an electrical signal within a semi-infinite cable. In our notation, the diffusion equation is

$$\frac{\partial^2 P}{\partial x^2} = a^2\frac{\partial P}{\partial t}, \qquad a^2 = \frac{\mu\beta\phi}{k}. \tag{10}$$

The parameter $a$ is the diffusivity, which depends on the viscosity $\mu$, the compressibility $\beta$, the porosity $\phi$, and the permeability $k$. The coordinate $x$ is measured inward from the boundary of the half-space.

Wylie shows that when starting with zero pressure everywhere in a semi-infinite body, when the pressure history at the boundary $P_0(t)$ is applied, then the pressure everywhere within the body is also known:

$$P(x,t) = \frac{ax}{2\sqrt{\pi}}\int_0^t P_0(t-\tau)\frac{\exp(-a^2x^2/4\tau)}{\tau^{3/2}}\mathrm{d}\tau. \tag{11}$$

Because we know $P(x,t)$ everywhere in the specimen, we can, in principle, calculate its gradient at the boundary $x = 0$ at any time $t$. Therefore, for an experiment performed on a semi-infinite (1D) specimen, given $P(t)$ and $V(t)$, we must then solve the following equation for the permeability $k$:

$$\frac{V}{P}\frac{\partial P}{\partial t} + \gamma\frac{\partial V}{\partial t} = -\frac{kA}{\mu}\left[\frac{d}{dx}\left(\frac{ax}{2\sqrt{\pi}}\int_0^t P(t-\tau)\frac{\exp(-a^2x^2/4\tau)}{\tau^{3/2}}\mathrm{d}\tau\right)\right]_{x=0}. \tag{12}$$

The exact form of the right-hand side of equation 12 is specific to the semi-infinite system, yet the approach to the problem is general, as discussed below.

*Linear system*

Regardless of the spatial derivative, the right-hand side of equation 12 is a convolution of the pressure history $P(t)$ with a system response function; i.e., it is an example of a constant parameter linear system (Bendat and Piersol, 1971). We can thus rewrite equation 12 as

$$Q(t) = \int_0^t P(t-\tau)h(\tau)\mathrm{d}\tau, \tag{13}$$

where $Q(t)$ is the net air flow into the cylinder (the left hand side of equation 12) and $h(\tau)$ describes the time response of $\nabla P|x = 0$ to a unit pressure impulse at the boundary. As is often done in analysis of linear systems, we can also consider the response of the system to the frequency content of the input signal. In the frequency domain, the response function $H(\omega)$ is related to the Fourier power spectra and cross-spectra $G$ of the inputs and outputs $P(t)$ and $Q(t)$:

$$G_Q(\omega) = |H(\omega)|^2 G_P(\omega), \tag{14}$$

$$G_{PQ}(\omega) = H(\omega)G_P(\omega), \tag{15}$$

where $\omega$ is the angular frequency. Aside from the frequency content of the driving signal, $H$ is a function of only constant parameters: the nozzle and specimen geometries and the physical properties of air and the specimen material ($\mu$, $\beta$, $\phi$, and notably the permeability $k$).

## Example of 1D finite-length sample

Consider flow through a perfectly jacketed, cylindrical sample with cross-sectional area $A$ and length $L$ (Figure 2). We suppose that one end, at $x = 0$, is kept at zero pressure, and the other end is subjected to a prescribed pressure $P_0(t)$ which starts at $t = 0$. We assume that in addition to prescribing, or at least knowing, the applied pressure $P_0(t)$, we can measure the instantaneous mass flow $Q(t)$ into the sample at $x = L$.

The gas pressure in the permeable sample $P(x, t)$ has to satisfy the flow equation 10, subject to the boundary and initial conditions,

$$P(x, t) = 0 \quad \text{for } t \le 0, \tag{16}$$

$$P(x = 0, t) = 0 \quad \text{for } t > 0, \tag{17}$$

$$P(x = L, t) = P_0(t) \quad \text{for } t > 0. \tag{18}$$

Equations 10 and 16–18 uniquely specify the flow history in the sample. If we can solve for this history $P(x, t)$, we can compute $Q(t)$ from (see equation 8)

$$Q(t) = -\frac{kA}{\mu}\left[\frac{\partial}{\partial x}P(x, t)\right]_{x=L}. \tag{19}$$

*Steady-state solution — Darcy's law*

One way to measure permeability with this system is to apply a constant pressure $P_0(t) = P_0$, a constant, and wait until $Q(t)$ has stabilized. We know that in equilibrium $\partial/\partial t \to 0$ and we will have

$$\frac{\partial^2 P}{\partial x^2} = 0. \tag{20}$$

The solution for pressure within the sample is

$$P(x, t) = \frac{x}{L}P_0, \tag{21}$$

where $P_0$ is the (constant) applied pressure. If we compute $Q$ and take the ratio $Q$ to $P_0$, we find

$$\frac{Q}{P_0} = -\frac{kA}{\mu L} = H, \tag{22}$$

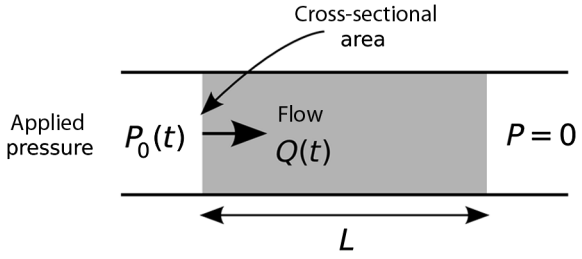


Figure 2. One-dimensional sample of length $L$ used in the example problem. Time-varying pressure $P_0(t)$ causes mass fluid flow $Q(t)$ into one end of the sample.

which is another form of Darcy's law (equation 8). By measuring the ratio $H$, we also know $k$, if we assume values for $A$, $\mu$, and $L$.

## A practical solution

In some situations, steady-state measurements are impractical, so we now examine the complete, time-dependent solution to find a way to measure $H$ that doesn't require equilibrium conditions.

Adopt the Fourier transform pair,

$$\tilde{f}(\omega) \equiv \int_{-\infty}^{\infty} f(t)e^{-i\omega t}\mathrm{d}t, \tag{23}$$

$$f(t) = \frac{1}{2\pi}\int_{-\infty}^{\infty} \tilde{f}(\omega)e^{i\omega t}\mathrm{d}\omega, \tag{24}$$

where we use $\tilde{f}$ to denote the Fourier transform of $f$. The Fourier-transformed version of the governing equation 1 is

$$\frac{\partial^2}{\partial x^2}\tilde{P}(x, \omega) = -i\omega a^2 \tilde{P}(x, \omega), \tag{25}$$

subject to the boundary and initial conditions,

$$\tilde{P}(x = 0, \omega) = 0, \tag{26}$$

$$\tilde{P}(x = L, \omega) = \tilde{P}_0(\omega). \tag{27}$$

The general Fourier-transformed solution is

$$\tilde{P}(x, \omega) = \frac{\sin(xa\sqrt{i\omega})}{\sin(La\sqrt{i\omega})}\tilde{P}_0(\omega). \tag{28}$$

Note that $\tilde{P}(0, \omega) = 0$ and $\tilde{P}(L, \omega) = \tilde{P}_0(\omega)$ as required by the boundary conditions. (If you plan to evaluate these expressions, note also that $\sqrt{i\omega}$ is a general, complex number, as are sines and cosines of it.)

The Fourier-transformed end flow is

$$\frac{\tilde{Q}(\omega)}{\tilde{P}_0(\omega)} = -\frac{kA}{\mu}a\sqrt{i\omega}\frac{\sin(xa\sqrt{i\omega})}{\sin(La\sqrt{i\omega})} = H(\omega). \tag{29}$$

If we compute this ratio in the zero-frequency limit, we find

$$\frac{\tilde{Q}(0)}{\tilde{P}_0(0)} = -\frac{kA}{\mu L} = H(0). \tag{30}$$

This looks like a restatement of equation 22 in which we defined $H$, but it is actually more general. From the definition of the Fourier transform, we know that

$$\tilde{f}(0) = \int_{-\infty}^{\infty} f(t)\mathrm{d}t, \tag{31}$$

so it follows that

$$H = \frac{\int_{-\infty}^{\infty} Q(t)\mathrm{d}t}{\int_{-\infty}^{\infty} P_0(t)\mathrm{d}t}. \quad (32)$$

This result is really interesting: If we take a sample that is initially quiescent, subject it to a pressure profile $P_0(t)$, which returns permanently to 0 after some interval, measure the flow profile $Q(t)$ until it returns to 0, and then sum each of those profiles and take the ratio of the two numbers, we will have measured (minus) $H$, which depends strongly on the sample permeability.

## IMPLEMENTATION

We have used the theory just described to build a practical device for measurement of rock matrix permeability or effective fracture apertures on outcrops and at the core scale (Figure 3; also see the Web site http://www.ner.com for a syringe permeameter built using this design). In this instrument, a soft circular rubber nozzle is affixed to a small air chamber containing an absolute air pressure transducer. This chamber is itself connected to a much larger variable volume cylinder (syringe) having an internal transducer for instantaneous measurement of the piston position and thus the total chamber air volume.

To use the device, the operator presses the rubber nozzle against the specimen and withdraws air from it with a single stroke of the syringe. The device is configured so that plunging the handle toward the sample draws a vacuum, a motion that keeps the nozzle in firm contact with the sample and helps to prevent leaks around the tip.

A battery-powered microcontroller unit records the transient absolute air pressure at the sample surface and the changing air volume within the syringe. The beginning and end of each measurement is sensed automatically from the operator's actions. Using signal-processing algorithms based on the theory described earlier (i.e., equation 31), the microcontroller computes the response function of the sample/instrument system $H$. The logarithm of the instantaneous value of this response function is displayed on the liquid crystal display along with the magnitude of the air pressure within the syringe body. Once the pressure inside the syringe returns to the ambient pressure (vacuum again reaches zero), the operator is signaled that the experiment is complete and the final value of the response function is noted on the display as a proxy for permeability.

As described earlier, theory shows that the response function is related to air permeability along with other (primarily geometrical) parameters. The requirement for explicit knowledge of the additional terms in the theory is avoided by empirical calibration of the device. As such, either matrix permeability or effective fracture flow aperture can be determined directly from empirical calibration charts determined for the instrument (Figure 4).

There are two sets of calibrations: (1) testing of a suite of five rocks, and (2) testing of parallel-plate "fractures." The five rock samples were a set of sedimentary rocks obtained from a source in Saudi Arabia and were a mixture of siltstones, sandstones, and carbonates of varied origin. The permeabilities used for each sample in the calibration were derived from a positive air-pressure gas permeability core scanner, whose calibrations relating gas to liquid permeability have been checked through standard petrophy-

Figure 3. Photographs of the syringe air permeameter.

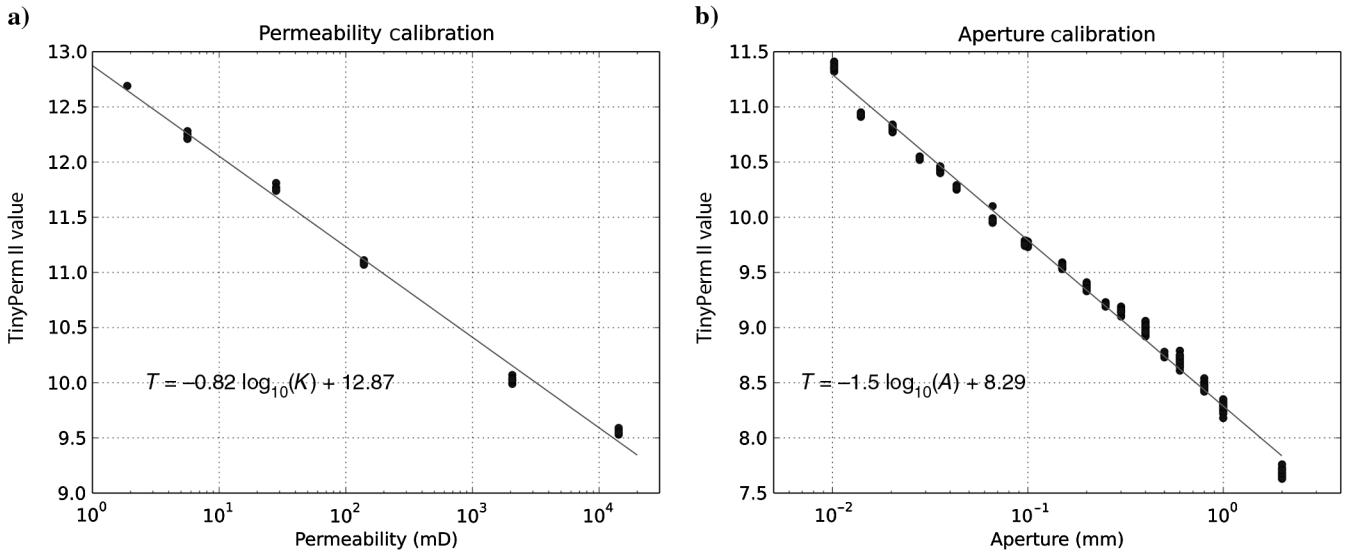


Figure 4. Empirical calibrations of the syringe permeameter for (a) matrix permeability and (b) fracture apertures. The commercial device, Tinyperm II, displays a value proportional to the logarithm of $H$ from equation 31. This value is shown on the $y$-axes.

sics tests in the laboratory. Repeated trials with the syringe permeameter for each of the five samples show on the calibration curve as scatter clustered tightly around the linear relationship on the calibration chart (Figure 4a).

The parallel-plate fracture calibration was done by separating two polished granite samples (standard flat machinist measurement plates) with known thickness feeler gauges. This calibration worked well, and the results were repeatable to a high degree, giving only tiny scatter about the linear relationship seen on the calibration chart (Figure 4b).

For intact rock, the matrix permeability measurement range with this device is from approximately 1 millidarcy (mD) to 10 darcys (D). Similarly, equivalent parallel-plate fracture apertures from approximately 20 μm to 2 mm can be determined.

The degree of linearity of the relationships shown in Figure 4 can be understood as follows. A linear least-squares fit for $x$ = (TinyPerm value) and $y = \log 10(\text{permeability})$ or $\log 10(\text{aperture})$ gives the coefficients as shown on the plots and in both cases gives coefficients of determination of $r^2 = 0.99$. The linear regression for $\log 10(\text{permeability})$ has a standard error of the estimate of $\sigma_{\log K} = 0.02$ and for the $\log 10(\text{aperture})$ has a standard error of $\sigma_{\log A} = 0.003$. Because linear distances separating points on a logarithmic scale represent ratios of the values, these standard errors represent at each measurement value an uncertainty of a factor of $10^{\sigma_K} = 1.05$ for permeability and a factor of $10^{\sigma_K} = 1.014$ for aperture. For example, if we have a 100-mD permeability rock sample, we might expect the instrument to show a value between 95 and 105 mD, but for a 1000-mD sample, the instrument might show a value between 950 and 1050 mD.

### *Case studies using the transient-flow syringe air permeameter*

This device has been used for several case studies documented in the literature. To provide a sense of the varied applications possible with such an instrument, we present a brief summary of those applications below.

Huysmans et al. (2008) describe the correlation of air permeability measurements made on a regular grid using the syringe permeameter to the underlying geology (Figure 5). This paper gives a detailed description of the measurements that were then used further in the paper described below concerning multiple-point geostatistics. Variograms of permeability and the anisotropy and heterogeneity of them were tied to cross-bedding structures. Here, the notion that small-scale structures strongly influence large-scale properties is illustrated.

Huysmans and Dassargues (2009) use the data described in the previous paper on the spatial variability of flow and transport properties to build training sets for multiple-point statistics. In this work, 2750 air permeability measurements were made on outcrops. Histograms, variograms, and the spatial distribution of permeability (heterogeneity and anisotropy) were analyzed in the context of overriding geologic descriptions, specifically, cross-bedded lithofacies.

Gribbin (2009) presents a study of permeability of rock from hydrothermal vents (locations of black smokers) sampled worldwide. The syringe permeameter was used to sample the variability of permeability among different rock types and horizons and to compare to permeability and porosity measured through other equipment on specific samples and as a function of confining pressure. Standard core permeability and air permeability measurements were made on the same rock, but on different subsamples. Both techniques were in general agreement, but the syringe permeameter allowed directional and position-specific sampling to be performed more efficiently directly in the field.

Fossen (2010) studies the difference between syndepositional and syntectonic deformation bands in sandstones and what the effects there are on permeability. This paper mentions, briefly, the use of the syringe permeameter to go along with core measurements on outcrop samples. It is not clear if the syringe permeameter was useful to the same extent as the core measurements were. Syntectonic bands can have marked permeability consequences, whereas syndepositional bands seem to have no effect within the measurement resolution of either technique, although they can be seen by the eye.

Monn (2006) performs a field study of a surface outcrop of a coastal sandstone gas reservoir in Utah. Part of the characterization was to map permeability variations among different facies including reservoirs and traps with bounding permeability barriers. When possible, plugs were taken and the permeability was measured in the lab, but in many cases, the friable nature of the sandstone prevented coring. The syringe permeameter was used for in situ measurements in these cases.

Plourde (2009) performs a study developing a discrete element model for granular porous media that relates cementation to permeability and elasticity. The syringe permeameter was used to scale the model results to the behavior of a real rock specimen, St. Peter Sandstone.

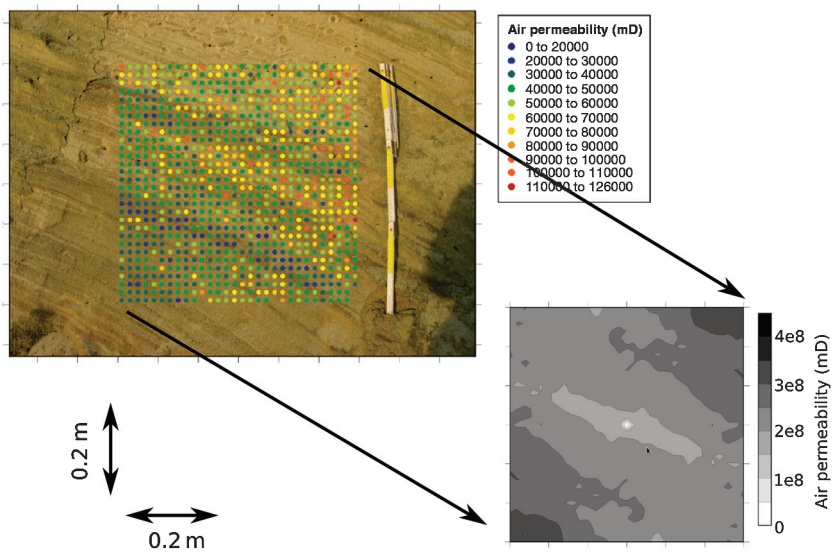


Figure 5. The outcrop study of heterogeneous permeability distribution of Huysmans et al. (2008). Air permeability was measured using the syringe permeameter on a dense regular grid (upper left), and the results were interpolated for use in geostatistical and flow modeling (lower right). Figure redrawn after Huysmans et al. (2008).

## CONCLUSIONS

Physical and chemical processes, including deposition, diagenesis, and mechanical deformation, create heterogeneity and anisotropy in rock and soil properties at all scales. Therefore, much recent effort has been placed on incorporating heterogeneity into numerical models of flow and transport. In these studies, the primary physical parameters of interest are the spatial variability of permeability and porosity.

In response to this need, we have designed and built a new portable field air permeameter to allow measurement of rocks in outcrop and on core. This has led to a commercial device capable of quantifying intact rock matrix permeability from approximately 1 mD to 10 D and for fractures quantifying the equivalent parallel-plate flow aperture from approximately 20 μm to 2 mm.

In this paper, we have described the underlying theory for the design and construction of this instrument and have briefly documented its use in field-scale studies of rock permeability heterogeneity.

## ACKNOWLEDGMENTS

We owe our thanks to R. Martin of New England Research, White River Junction, Vermont, USA, for his support of this work from the prototype stages to the commercialization of TinyPerm II.

## REFERENCES

Bendat, J. S., and A. G. Piersol, 1971, Random data: Analysis and measurement procedures: Wiley-Interscience, 136–141.

Castle, J. W., F. J. Molz, S. Lu, and C. L. Dinwiddie, 2004, Sedimentological and fractal-based analysis of permeability data, John Henry Member, Straight Cliffs Formation (Upper Cretaceous), Utah, USA: Journal of Sedimentary Research, **74**, 270–284, doi: 10.1306/082803740270.

Dagan, G., 1986, Statistical theory of groundwater flow and transport: Pore to laboratory, laboratory to formation, and formation to regional scale: Water Resources Research, **22**, 120S–134S, doi: 10.1029/WR022i09Sp0120S.

Dreyer, T., A. Scheie, and O. Walderhaug, 1990, Minipermeameter-based study of permeability trends in channel sand bodies: AAPG Bulletin, **74**, 359–374.

Dykstra, H., and R. L. Parsons, 1950, The prediction of oil recovery by waterflood, *in* H. Dykstra, and R. L. Parsons, eds., Secondary recovery of oil in the United States: Principles and practice, 2nd ed.: American Petroleum Institute, 160–174.

Fossen, H., 2010, Deformation bands formed during soft-sediment deformation: Observations from SE Utah: Marine and Petroleum Geology, **27**, 215–222, doi: 10.1016/j.marpetgeo.2009.06.005.

Goggin, D. J., M. A. Chandles, G. Kocurek, and L. W. Lake, 1988a, Patterns of permeability in Eolian deposits: Page Sandstone (Jurassic), NE Arizona: SPE Formation Evaluation, **3**, 297–306, doi: 10.2118/14893-PA.

Goggin, D. J., R. L. Thrasher, and L. W. Lake, 1988b, A theoretical and experimental analysis of minipermeameter response including gas slippage and high velocity flow effects: In Situ, **12**, 79–116.

Gribbin, J., 2009, Insights into deep-sea hydrothermal vent environments from measurements of permeability and porosity: Student Paper GEOL 394H, University of Maryland, http://www.geol.umd.edu/undergraduates/paper/paper_gribbin.pdf, accessed 5 April 2013.

Hartkamp, C. A., J. Arribas, and A. Tortosa, 1993, Grain-size, composition, porosity and permeability contrasts within cross-bedded sandstones in Tertiary fluvial deposits, central Spain: Sedimentology, **40**, 787–799, doi: 10.1111/j.1365-3091.1993.tb01360.x.

Hurst, A., and D. J. Goggin, 1995, Probe permeametry: An overview and bibliography: AAPG Bulletin, **79**, 463–473.

Huysmans, M., and A. Dassargues, 2009, Application of multiple-point geostatistics on modeling groundwater flow and transport in a cross-bedded aquifer (Belgium): Hydrology Journal, **17**, 1901–1911, doi: 10.1007/s10040-009-0495-2.

Huysmans, M., L. Peeters, G. Moermans, and A. Dassargues, 2008, Relating small-scale sedimentary structures and permeability in a cross-bedded aquifer: Journal of Hydrology, **361**, 41–51, doi: 10.1016/j.hydrol.2008.07.047.

Iversen, B. V., P. Moldrup, P. Schjønning, and O. H. Jacobsen, 2003, Field application of a portable air permeameter to characterize spatial variability in air and water permeability: Vadose Zone Journal, **2**, 618–626, doi: 10.2113/2.4.618.

Jacobsen, T., and H. Rendall, 1991, Permeability patterns in some fluvial sandstones. An outcrop study from Yorkshire, northeast England, *in* L.W. Lake, H. B. Carroll, Jr, and T. C. Wesson, eds., Reservoir characterization II: Academic Press, 315–338.

Jensen, J. L., C. A. Glasbey, and P. W. M. Corbett, 1994, On the interaction of geology, measurement, and statistical-analysis of small-scale permeability measurements: Terra Nova, **6**, 397–403, doi: 10.1111/j.1365-3121.1994.tb00513.x.

Koltermann, C. E., and S. M. Gorelick, 1996, Heterogeneity in sedimentary deposits: A review of structure-imitating, process-imitating, and descriptive approaches: Water Resources Research, **32**, 2617–2658, doi: 10.1029/96WR00025.

Monn, W. D., 2006, A multidisciplinary approach to reservoir characterization of the coastal Entrada erg-margin gas play, Utah: M.S. thesis, Brigham Young University.

Plourde, K. E., 2009, Quantifying the effects of cementation on the hydromechanical properties of granular porous media using discrete element and poroelastic models: M.S. thesis, University of Massachusetts.

Tidwell, V. C., and J. L. Wilson, 1999, Upscaling experiments conducted on a block of volcanic tuff: Results for a bimodal permeability distribution: Water Resources Research, **35**, 3375–3387, doi: 10.1029/1999WR900161.

Wylie, C. R., 1975, Advanced engineering mathematics, 4th ed.: McGraw-Hill, 385–386.

Zemansky, M. W., 1968, Heat and thermodynamics, 5th ed.: McGraw-Hill, 111–144.